Laboratory experiments on large-scale geophysical flows

Miklós Vincze [*‡] and Imre M. Jánosi [†‡]

[*] MTA-ELTE Theoretical Physics Research Group, Budapest, Hungary

[†] Department of Physics of Complex Systems, Eötvös Loránd University, Budapest, Hungary

[‡] von Kármán Laboratory for Environmental Flows, Eötvös Loránd University, Budapest, Hungary

1 Historical Overview

Laboratory experiments have been playing a unique role in the great scientific endeavor to better understand the complex phenomena of environmental flows for centuries. Thus, we find it quite appropriate to start our review – motivated by an Italian conference and written by Hungarian authors – with a historic reference to the heritage of the 17th century scholar Luigi Fernando *Marsigli* (1658–1730), native of Bologna. Being eminent in all areas of contemporary science ranging from mathematics to anatomy, he was commissioned to carry out the complete cartographic and zoological survey of the border area between the Kingdom of Hungary and the Ottoman Empire: a task that made him spend twenty years of his life roaming in and around Hungary. His visit to Constantinople (now Istanbul, Turkey) inspired his later pioneering work on the physical background of seawater exchange through the strait of Bosporus. He assumed that the reported undercurrent from the Mediterranean towards the Black Sea is driven by the density difference between the two basins due to the higher salinity of Mediterranean seawater. Marsigli demonstrated this idea in an experimental tank which he divided into two sections by a vertical wall in the middle (Figure 1b). The two sections were filled with saline- and freshwater and one side was painted with ink for visualization (Marsigli, 1725). The flow was then initiated by opening two holes at the top and bottom of the separating wall, leading to the formation of a saline front at the bottom and an opposing freshwater front at the top. Marsigli's hypothesis (and its demonstration) has led to the theory of buoyancy-driven environmental flows and eventually to the foundation of physical oceanography. The two-box experimental configuration itself has also become one of the standard

A. Provenzale et al. (Eds.), *The Fluid Dynamics of Climate,*
CISM International Centre for Mechanical Sciences
DOI 10.1007/ 978-3-7091-1893-1_3

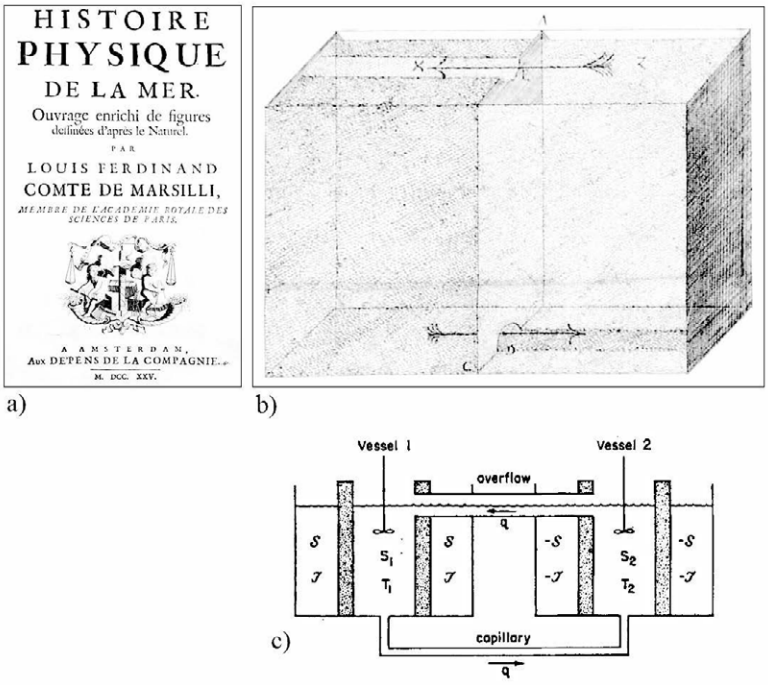

Figure 1. (a) The cover of probably the very first book on physical oceanography, Marsigli's "Histoire physique de la mer", translated to French by Leclerc (Amsterdam, 1725). (b) The schematic drawing of Marsigli's two-box experimental set-up from the book. (c) The sketch of Henry Stommel's famous conceptual model of the meridional overturning from his original paper (Stommel, 1961).

conceptual tools in the field to this day: the theoretical study of the fluxes in a similar set-up with additional differential heating provided the first qualitatively correct insight into the dynamics of the meridional overturning ocean circulation in the groundbreaking works (e.g., (Stommel, 1961)) of Henry *Stommel* (1920–1992), see Figure 1c.

Revealing the pathways of heat exchange and thermal mixing in the overturning currents keeps oceanographers busy even nowadays. One of the most cited papers on these issues also happens to be an experimental work, that of Swedish oceanographer Johan *Sandström* (1874–1947) from 1908

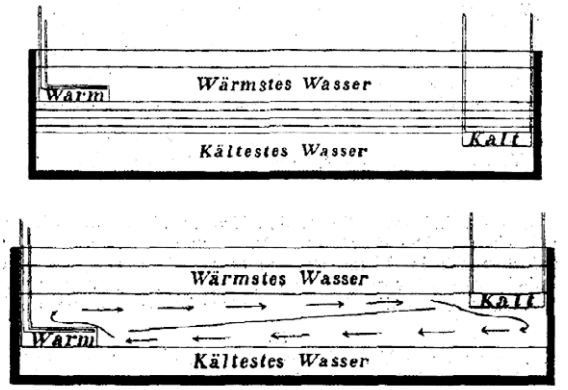

Figure 2. Two sketches from the original paper of J. Sandström on his ocean circulation experiment (Sandström, 1908). According to his 'theorem', if the heat source is at higher level than the heat sink (top) the fluid stays at rest, and overturning can by initiated only if the configuration is reversed (bottom).

(Sandström, 1908). In this study the author investigated how the relative vertical position of a heat source and a heat sink affects the flow properties in a rectangular tank of saline water. He reported that an overturning flow could only be initiated if the heat source was placed *below* the level of the cooling source (sink), as shown in Figure 2, reproduced from the original paper. This conclusion has become known as Sandström's 'theorem' and has been widely disputed in the past century, due to its controversial oceanographic implications. Clearly, the Atlantic meridional overturning circulation does exist, despite being driven by the differential incoming Solar heat fluxes between the equatorial and polar regions, which both act at the water surface, i.e. at the same geopotential level, virtually violating the 'theorem'. Although a recent study has found Sandström's results inconsistent with those of a reconstructed experiment (Coman et al., 2006), yet the work's impact is undeniable: to circumvent the violation of the 'theorem', researchers have uncovered various possible ways of heat and momentum transfer in the ocean, from localized geothermal heat sources (Vincze et al., 2011b) to tidally excited internal waves (Zhang et al., 2008).

The first experimental demonstration of such large-amplitude internal waves that propagate in the bulk of the stratified ocean while remaining

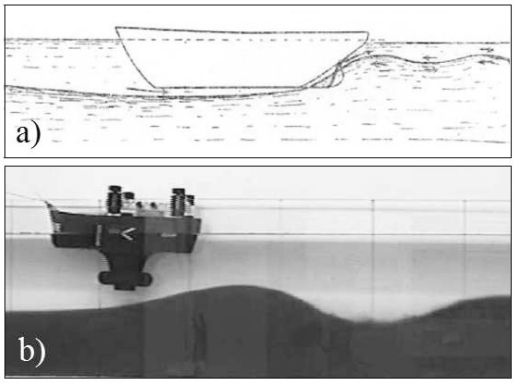

Figure 3. (a) A schematic drawing of internal wave excitation behind a ship model from Ekman's original paper (Ekman, 1904). (b) The experiment repeated a hundred years later in the von Karman Laboratory, Budapest.

practically unnoticed from the surface has been conducted by Sandström's fellow citizen and contemporary, Vagn Walfrid *Ekman* (1874–1954). Ekman was given captain Nansen's logs on the 1893-96 Arctic expedition of the legendary research ship Fram. Nansen wrote: "When caught in dead water Fram appeared to be held back, as if by some mysterious force, and she did not always answer the helm. In calm weather, with a light cargo, Fram was capable of 6 to 7 knots. When in dead water she was unable to make 1.5 knots." (Walker, 1991). By towing a model of the ship in a laboratory tank filled with stratified water (Figure 3), Ekman realized that this motion excites large waves in the bulk at the internal density interfaces, to which the model ship loses its kinetic energy, hence, speed (Ekman, 1904). This demonstration paved the way for the research of flow-topography interactions in stratified media. It is also interesting to note that Nansen's very same notebook contained the descriptions of the drift of icebergs as well, which motivated Ekman's discovery of the Ekman spiral, a contribution that has clearly made him one of the founding fathers of modern oceanography and meteorology.

Besides stratification, the other important unique feature that distinguishes geophysical hydrodynamics from the everyday 'human-scale' fluid mechanics is the dominant role of Coriolis force. A surprisingly large part of the complexity of atmospheric and ocean dynamics at the mid-latitudes can be attributed to the interplay of the planetary rotation (yielding Coriolis

effect) and the horizontal buoyancy (temperature and/or salinity) gradients. The first experimental 'minimal model' of atmospheric circulation based on these principles was constructed by German meteorologist and medic Friedrich *Vettin* (1820–1905) in 1857. He studied the flow patterns of cigar smoke in an air-filled rotating cylindrical container, in which radial temperature gradient was introduced by a block of ice placed at its center (Vettin, 1884), representing the cold polar regions of Earth. Vettin observed convective vortices, but the applied model parameters (size, rotation rate, temperature gradient) did not allow the exploration of flow regimes outside the 'sideways-convective' axially symmetric overturning state (also known as Hadley regime).

These pioneering studies and the similar ones that followed in the first half of the 20th century (Fultz, 1949, 1952) of rotating convective flows were rather qualitative in nature and their experimental circumstances and procedures were hard to control and replicate. Yet, the same period brought forth the first systematic laboratory studies which could be *quantitatively* compared with linear stability analyses in the field of rotating fluids, namely the classic works of Sir Geoffrey Ingram *Taylor* (1886–1975) on the cylindrical Couette flow (Taylor, 1923). It was not until the 1950s when the differentially heated and rotating configuration was investigated to such detail and precision by the team of David *Fultz* (1921–2002) in Chicago and, in parallel, the young Raymond *Hide*, then graduate student in Cambridge (UK). In his PhD thesis, Hide gave the first description of periodic waves, analogous to the large-scale planetary waves in the atmosphere, in an annular rotating tank filled with water, cooled at the inner cylindrical sidewall and heated at the outer rim (see Figure 4). As remarked by Ghil et al. (2010), the thesis also contained "one of the first, or maybe *the first*, study of what we call today bifurcation and regime diagrams in a fluid dynamical context". The insight provided by these experiments into the basic underlying dynamics of atmospheric circulation had a very powerful impact on the formulation of theoretical and numerical minimal models (conceptual, or 'toy models') of the atmosphere, i.e. the ones constructed by Edward Norton *Lorenz* (1917–2008), see e.g. Lorenz (1963); the experiments have clearly demonstrated which factors are truly essential for an 'irreducible' description of the basics of mid-latitude atmospheric flows, and which ones can be omitted. It turned out that for a minimal model of cyclogenesis or jet stream formation one does not need to consider the role of topography, evaporation, precipitation or even the curvature of the surface, only the meridional temperature difference and the Coriolis effect (Lorenz, 1967).

This approach of creating environmentally inspired conceptual laboratory models has been flourishing since then: currently active research topics

range from modeling the interactions between internal waves and various seafloor topographies (Zhang et al., 2008; Boschan et al., 2012) to the experimental exploration of "meddy" formation in rotating stratified media (Aubert et al., 2012), wave attractors of inertial and gravity waves (Klein et al., 2014) or the conceptual demonstration of the famous hexagonal vortex at the north pole of planet Saturn, just to pick a random selection, in which all studies share the main principle of the above listed historic experimental works: making the model of the given phenomenon "as simple as possible, but no simpler".

Inspired by the fascinating property of nature that planet-scale hydrodynamic phenomena can be properly modeled using tabletop-size setups in a relatively inexpensive way, and the perspective that even physical oceanographic problems can be addressed in a completely land-locked country, triggered the foundation of the *von Karman Laboratory of Environmental Flows* at the then-new campus of the Eötvös University (Budapest, Hungary) in 2000. Of course, in terms of instrumentation, the aim of our laboratory has never been to compete with the impressive capabilities of the handful of major institutions in Europe (e.g. the Geophysical Fluid Dynamics Lab of the Department of Physics in Oxford, or the 13 m-wide Coriolis Platform in Grenoble, where all measurement devices and even the experimenters can co-rotate with their set-ups). Nevertheless, our experience of the past decade has clearly shown that there is a lot to discover in this – surprisingly young – field of classical physics, where even the simplest experiments can yield useful insight into the underlying dynamics of environmental flows, if one looks carefully enough. In the present review, after giving a brief introduction into the principles that make such modeling possible, we present a few 'case studies' selected among our more recent results to demonstrate the diversity and efficiency of this experimental approach and the ways it can contribute to our better understanding of the climate system.

2 The basics of laboratory modeling

For a brief mathematical demonstration of the principle of *hydrodynamic similarity*, let us consider the Navier-Stokes equation of an incompressible flow, as observed from a rotating system:

$$\frac{d\vec{v}}{dt} = -2\vec{\Omega} \times \vec{v} - \frac{1}{\rho}\nabla p - \vec{n}g + \nu\nabla^2\vec{v}. \tag{1}$$

Here $\vec{\Omega} \equiv \Omega\vec{n}$ denotes the angular velocity vector of the reference frame (co-aligned with the vertical unit vector $\vec{n}$), $\vec{v}$ is the velocity vector, ρ and ν represent the density and kinematic viscosity of the fluid parcel, respectively,

g represents the gravitational acceleration and p is the pressure field. The form $d\cdot/dt \equiv \partial\cdot/\partial t + \vec{v}(\nabla\cdot)$ on the left hand side denotes the advective time derivative.

One can now rescale the equation by setting the linear size L of the considered domain, and the flow's characteristic (e.g., mean) velocity U as 'natural' units. These transformations can be expressed formally as replacements $\vec{r} \to L\vec{r}$ ($\vec{r}$ being the position vector) and $\vec{v} \to U\vec{v}$. Combining the new length and velocity units yields our natural timescale: $t \to L/U\,t$. Though not that manifestly, but one can easily get the corresponding transformation of the pressure units as well (for details we refer to, e.g. Vallis (2006)) in the form of $p \to 2\rho|\Omega|LU\,p$. After carrying out these replacements and dividing the equation by the scale factor U^2/L of the rescaled derivative at the left-hand side we arrive at the following re-organized form:

$$\frac{d\vec{v}}{dt} = -\frac{1}{Ro}(\pm\vec{n}\times\vec{v} + \nabla p) - \frac{1}{Fr^2}\vec{n} + \frac{1}{Re}\nabla^2\vec{v}, \tag{2}$$

where Rossby number $Ro \equiv U/(2|\Omega|L)$ quantifies the characteristic ratio of hydrodynamic acceleration and Coriolis acceleration (the appearance of $\pm$ is a consequence of defining Ro with the absolute value of the angular velocity). Similarly, Froude number $Fr \equiv U/\sqrt{gL}$ accounts for the relative magnitude of gravitational acceleration, and Reynolds number $Re \equiv UL/\nu$ measures the importance of the viscous acceleration in the same manner. It is to be emphasized that these products are dimensionless pure numbers.

Two flows are considered dynamically similar if – besides the geometric similarity of the set-ups – their dimensionless numbers match. Note, that it is generally not possible to fulfill perfect similarity in terms of *all* parameters, unless the two considered systems are identical. However, in most of the applications many terms can be neglected. For the vast majority of engineering-oriented applications the Coriolis force does not play any role ($Ro \to \infty$), and the effect of gravity (hydrostatic pressure) can be absorbed into the pressure term. Thus, for a wind-tunnel test of a car model, Reynolds number Re is the only relevant, and perfectly sufficient, parameter of dynamic similarity. For a ship model in an open channel flow, however, both viscous drag (quantified via Re) and gravity wave emission at the water surface (scaling with Fr) dissipate some of the model's kinetic energy. In this case both forces are of relevance, and the full similarity could only be achieved (if at all) by using fluids of different viscosities in the model and the prototype (Kundu and Cohen, 2008).

Fortunately, changing the medium is not the only possible way to circumvent such difficulties. Laboratory experiments can still be useful even without reaching perfect similarity, if one is able to separate the differently

scaling effects and apply corrections accordingly. For example, in the above case, the viscous drag acting on the ship model can be measured alone in a control experiment, where the surface wave excitation is somehow inhibited (e.g. by placing a rigid lid at the top of the tank), and therefore only the value of Re remains relevant. By subtracting this result from the drag of the original experiment, one can separate the contribution of the emitted surface waves, and this difference can be readily compared to the large prototype.

For planet-scale flows, the first term of (2) predominates ($Ro \to 0$). The stationary solution of the governing equation (2) in this limit can be obtained by omitting the gravitational and viscous terms ($Fr \to \infty$ and $Re \to \infty$) and setting the left hand side to zero. In this case, referred to as *geostrophic equilibrium*, pressure perturbations are balanced by stationary flow *along* the isobars. In environmental flows, generally, the larger the considered length scale is, the better this approximation becomes, as the characteristic values of Ro drop. For example, in case of a cyclone with a linear size $L = 1000$ km and wind speed $U = 10$ m/s the formula yields $Ro \approx 0.07$, and can be even two or three orders of magnitude smaller for meddies (i.e. isolated vortex lenses in the salty Mediterranean water). As a comparison, for a bathtub drain (with $U = 0.1$ m/s and $L = 0.1$ m), one gets ca. $Ro \approx 6850$. Thus, by taking a quick look at (2), it is immediately visible, that the widespread rumors about bath drain flows circulating opposite ways on the Northern and Southern hemispheres due to Coriolis effect have no basis at all: besides the characteristic values of Fr and Re of the same flow, this effect is completely negligible. However, by placing the same bathtub flow onto a turntable with an angular velocity $\Omega = 7$ rad/s (about one rotation per second), one can arrive at the 'cyclonic' value of Ro in laboratory scale, making it relatively easy to achieve hydrodynamic similarity in a rotating model flow.

Obviously, the governing equation (2) is not sufficient for a complete physical description of the flow in itself. In case of a large-scale environmental flow, the thermal boundary conditions and the 'equation of state' – here, the relationship $\rho(T)$ between the density and temperature of the fluid parcels – are of fundamental importance just as well. A convenient nondimensional combination for quantifying all these factors in a rotating thermal convection driven by a horizontal temperature gradient is a special version of Ro. It is known as thermal Rossby number Ro_T (or Hide number), and defined as

$$\mathrm{Ro}_T = \frac{\alpha g H \Delta T}{(2\Omega)^2 L^2} \ , \tag{3}$$

where α is the coefficient of volumetric thermal expansion for the fluid and ΔT is the temperature contrast imposed at the vertical boundaries of the rotating layer.

The thermal Rossby number has a fairly transparent explanation by considering the aforementioned case of geostrophic equilibrium. Expressing the relevant terms of (2) in cylindrical coordinates, the zonal velocity component u_θ is determined by the radial pressure difference as

$$u_\theta = -\frac{1}{\rho_0 2\Omega}\frac{\partial p}{\partial r} \ , \tag{4}$$

where ρ_0 is a mean density of the fluid at a reference temperature T_0, and friction is neglected. The pressure difference is a consequence of radial temperature contrast inducing a change in density $\Delta\rho = -\alpha\rho_0\Delta T$. Using the hydrostatic approximation $p = \rho g H$, the radial pressure difference in a shallow layer can be estimated as $\Delta p = -\alpha\rho_0 g H \Delta T$, which gives an estimate to a relative velocity scale

$$U_T = \frac{\alpha g H \Delta T}{2|\Omega|L} \ . \tag{5}$$

A simple comparison with Eq. (3) reveals that the thermal Rossby number is in full analogy with the "regular" one, since it is given as the ratio of two characteristic velocity scales:

$$\mathrm{Ro}_T = \frac{U_T}{2|\Omega|L} \ . \tag{6}$$

We note, that when the horizontal temperature difference ΔT is comparable to the vertical one, i.e. $\Delta T_z \approx \Delta T$ holds, Ro_T is proportional to the Burger number Bu, defined as the squared ratio of the Rossby deformation radius $R_d = \sqrt{gH\alpha\Delta T_z}/\Omega$ to the linear size L; $Bu = gH\alpha\Delta T_z/(\Omega^2 L^2)$.

As we will soon see, Ro_T is not the only relevant parameter to characterize thermally driven rotating flows, yet, it clearly demonstrates the power of hydrodynamic similarity: by adjusting the thermal boundary conditions, geometric properties and the rotation rate in a model setup, it is possible to access various spatial and temporal scales of the atmospheric and oceanic flows, even to model atmospheric features of other planets in the solar system, see e.g. Mitchell et al. (2015).

3 Case studies

In the section that follows four current or recent experimental research topics of the authors will be introduced and briefly discussed, all of which are

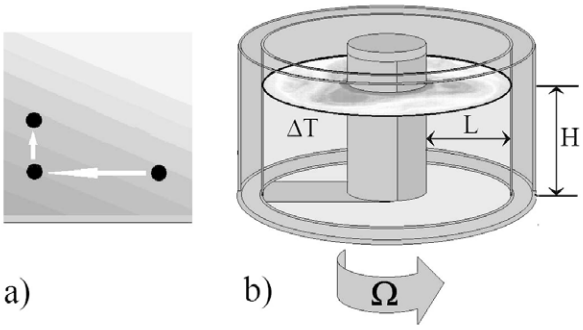

Figure 4. (a) A conceptual sketch of baroclinic unstable fluid parcel displacement through sloping isothermal levels. (b) A schematic drawing of a baroclinic wavetank with the most important geometrical and physical parameters.

related to problems of thermally driven rotating environmental flows. We selected these case studies so that they can hopefully give the reader an impression of the diversity of phenomena that can be studied by using slightly different variants of practically the same experimental configuration.

3.1 Baroclinic instability and inertia-gravity waves

Without the effect of rotation, the constant density levels in a stably stratified system would be perfectly horizontal. In geostrophic equilibrium, however, winds blowing perpendicular to the plane of the local density gradient can stabilize tilted stratification – a direct consequence of equation (4). This process can also act the other way: if constant heat fluxes at the vertical boundaries maintain a sloping a stratification in a rotating system, an out-of-plane meanflow, the so-called *thermal wind* will develop. Within the framework of the geostrophic theory, one can easily obtain a connection between windspeed U and the slope s_T of isotherms (see, e.g. Vallis (2006)) in the form of

$$s_T = \frac{2|\Omega|U}{g\alpha\Delta T}. \tag{7}$$

If s_T is large enough, a fluid parcel, displaced by an initial perturbation parallel to the (flat) bottom boundary, though traveling along an equipotential, may reach a region of higher density (Figure 4a). From here, the buoyancy force lifts the parcel until it reaches its original isotherm – at a

larger geopotential. Apparently, a small perturbation yields a larger displacement, thus this flow is unstable; the phenomenon is hence coined *baroclinic instability*. This 'surplus' potential energy is released in the form of kinetic energy, and excites baroclinic (planetary) waves, the main sources of cyclogenesis in the mid-latitude atmosphere. Besides Ro_T the kinematic viscosity ν of the medium also plays an important role in this instability; it introduces a 'viscous cutoff' that dissipates too weak thermal winds and also damps the instability of too large wavenumbers. This effect is parametrized by Taylor number Ta that accounts for the ratio of rotational and viscous effects, and reads as

$$Ta = \frac{4\Omega^2 L^5}{\nu^2 H}. \tag{8}$$

Ro_T and Ta are thus used together to characterize the different dynamical regimes in rotating, thermally driven systems, such as planetary atmospheres, oceanic basins and their minimal models in the laboratory. A typical experimental configuration is depicted in Fig.4b: the tank consists of co-rotating coaxial cylinders. The innermost cylinder (representing the polar region) is cooled whereas the outer rim is heated, thus the working fluid in the middle annular gap experiences temperature difference ΔT. Traditionally, for this experimental set-up the width of the gap (i.e. the difference of its inner and outer radii) is used as characteristic length L.

In Figure 5 we present a sketch of the regime diagram (after Hide (1953)) defined by the two nondimensional numbers. The insets (labelled with letters a-e) show examples of the typical flow patterns of the different regimes. The Ta and Ro_T values corresponding to the insets are highlighted in the regime diagram. Figure 5a is a composite satellite image of Earth's southern hemisphere as seen from the direction of its axis (with Antarctica in the middle). The irregularly shaped cyclonic and anticyclonic eddies of Earth's atmosphere are visibly quite similar in structure to those obtained via infrared thermography of the rotating annulus at the Brandenburg Technical University (BTU) Cottbus, Germany, at similar values of Ta and Ro_T (Figure 5b). Decreasing Ta and increasing Ro_T simultaneously by two orders of magnitude brings the system to the regime where the velocity and temperature fields exhibit persistent regular waves that propagate along the azimuthal direction in the tank due to baroclinic instability. Figure 5c shows a typical snapshot of such a pattern with dominant wavenumber (i.e. the number of lobes) $m = 3$ in the annulus. Figure 5d and e show the axisymmetric structures that develop when further decreasing Ta and increasing Ro_T. The former one is, again, a thermographic snapshot of the annulus, whereas the latter is a spacecraft image of the atmosphere of planet Venus, well known for its slow rotation (one revolution takes 243 Earth days). It

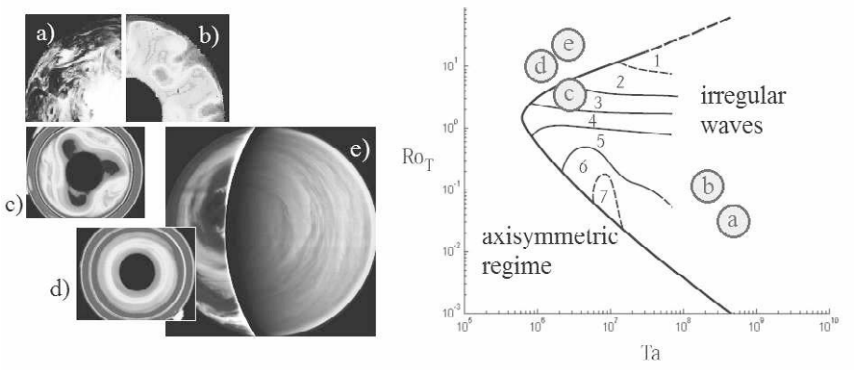

Figure 5. The schematic regime diagram of thermally driven rotating flows, defined by Taylor and Rossby numbers. The numbers indicate the azimuthal wavenumbers of baroclinic waves along the circumference of the tank for the 'regular wave' regime. The insets: the mid-latitude atmosphere of Earth (a), thermographic images of the BTU rotating annulus setup at the different flow regimes (b-d) and a composite image of Venus' atmosphere; the sun-lit side in visible, the night side in infrared wavelength range (Source: ESA).

can be generally stated that for large values of Ta (far from the 'viscous cutoff'), in case of $Ro_T \gg 1$, the flow is axisymmetric and not significantly disturbed by rotation (as in the Venusian atmosphere), whereas for $Ro_T \ll 1$ the dynamics is dominated by the Coriolis effect.

As briefly mentioned in the historical overview, internal (gravity) waves play an important role in heat and momentum transport both in the oceans and the atmosphere. In a stably stratified system, a fluid element with reference density ρ_0 displaced vertically from height z, keeping its density, oscillates at buoyancy- (or Brunt–Väisälä-) frequency $N(z) = \sqrt{g\rho_0^{-1}\,|d\rho(z)/dz|}$. Gravity waves can be understood as propagating buoyancy oscillations in the medium. These 'ripples' are widely known to be generated by flow-topography interactions (lee waves in the atmosphere or tidal conversion above mid-ocean ridges). Yet it has been noticed just recently by meteorologists (Ghil et al., 2010) that similar waves are also excited in the vicinities of the large-scale baroclinic cyclones without any topographic obstacle, and they are increasingly recognized as significant sources of uncertainty in weather forecasting. Strictly speaking, these waves are not pure gravity waves, since the Coriolis effect (inertial motion) also affects their propaga-

tion. Such "hybrid" combinations of the two wave types are referred to as inertia-gravity waves (IGWs), and their nontrivial dispersion relation has the form of

$$\omega^2 = N^2 \cos^2 \zeta + f^2 \sin^2 \zeta, \tag{9}$$

where the angular frequency ω of the wave is determined by the aforementioned N, the Coriolis frequency $f \equiv 2\Omega \sin \vartheta$ (Ω being the angular frequency of the rotation of Earth and ϑ the geographic latitude), and $\zeta \equiv \arctan(n/\sqrt{k^2 + l^2})$, the angle of phase propagation relative to the horizontal plane, set by horizontal wavenumbers k, l and vertical wavenumber n. Nonlinear interactions between baroclinic waves, spontaneous imbalance and geostrophic adjustment are all possible sources of IGWs in such a system. It is important to note that the scale difference between these waves and the large planetary waves that excite them is very large, making the coupling very difficult to resolve in numerical models. Thus laboratory experiments appear to be useful test-beds to better understand these phenomena, even though perfect hydrodynamical stability can hardly be reached in such a multiscale system.

In the upper troposphere of the mid-latitudes the ratio of N/f is approximately on the order of $\mathcal{O}(100)$, whereas for a typical rotating annulus experiment (in the regime of baroclinic instability) with parameters $L \approx H \approx 0.1$ m, $\Omega \approx 5$ rpm and $\Delta T \approx 10$ K typically $N/f \sim \mathcal{O}(0.1)$ holds (Borchert et al., 2014). Taking a glimpse at equation (9) it becomes obvious that this difference is not just quantitative but also qualitative: in the atmosphere, the high frequency waves propagate nearly horizontally (and the low frequencies vertically), whereas in this classic laboratory set-up the behavior is just the opposite.

There have been several attempts and suggestions to create a more 'atmosphere-like' experimental apparatus, based on the rule of thumb that in such rotating systems where the isothermal surfaces are tilted, the total vertical difference ΔT_z is comparable to its horizontal counterpart ΔT. Decreasing fluid depth H and increasing ΔT both tend to raise the vertical temperature gradient, and thus N, which can be estimated from $N^2 \approx g\alpha\Delta T/H$. However, the water layer cannot be arbitrarily shallow either, because then the boundary layers at the horizontal lids (e.g. the Ekman layers) would invade the flow too much and modify the dynamics markedly. Also, care must be taken not to suppress baroclinic instability, meaning that the geometrical parameters and the boundary conditions must be set so to keep the system within the baroclinic unstable regime of the $Ta - Ro_T$ plane (see Figure 5). For example if f (that is $f = 2\Omega$ for a laboratory tank) were set too small, then the flow would be axially symmetric and no planetary waves would be present to excite IGWs.

In their recent work, Borchert et al. (2014) from the Goethe University of Frankfurt am Main, suggested a wide and shallow configuration ($H = 4$ cm, $L = 50$ cm, $\Omega = 0.78$ rpm, $\Delta T = 30$ K) to yield at least $N > f$ on average. This tank is currently under construction at the Brandenburg Technical University within the framework of the MS-GWaves program, dedicated to the numerical, experimental, and observational investigation of IGWs. In this apparatus the large vertical aspect ratio L/H may lead to difficulties, due to the significant heat exchange occurring between the large horizontal surface of the working flow and the (supposedly insulating) horizontal lids.

Another way to increase N is introducing vertical salinity gradient to the set-up. This method was applied within the framework of a joined German-French-Hungarian collaboration (involving Patrice *Le Gal* of U. Aix-Marseille, Uwe *Harlander* of BTU Cottbus and the authors). A continuously stratified salinity profile was prepared in the experimental cavity before each measurement with the so-called double-bucket technique (Oster and Yamamoto, 1963) two vessels containing saline and fresh water are connected via a pipe so that the freshwater inflow to the saline bucket yields a mixture of ever decreasing salinity in time. By raising or lowering one of the buckets during this filling-up procedure, we were able to adjust the water fluxes into the mixing compartment and, thus, create arbitrarily non-uniform stable salinity profiles.

Imposing lateral temperature and vertical salinity gradients in the same set-up can lead to the formation of *double diffusive convection* (Chen et al., 1971). However, at depths where the salinity stratification is steep enough to make the parameter $\eta \equiv \alpha \Delta T/(d\rho/dz)$ smaller than a critical ratio η^*, the fluid stays at rest: the large gradient inhibits the overturning convection to penetrate the full depth of the bulk, and confines baroclinic instability into a shallower layer, where $\eta > \eta^*$ holds. Therefore the effect of salinity stratification is twofold. Firstly, it directly increases N. Secondly, with reducing the effective H to the vertical domain of the convective layer, it keeps the system baroclinic unstable for smaller values of f as well (note that both Ta and Ro_T scale with Ω^2/H, thus one can trade rotation rate for water depth and still stay in the same flow regime). Moreover, this shallow layer is practically free from the undesirable boundary layer effects, since it can be set 'floating' at any water level, depending on the prepared salinity profile only, without any direct thermal or mechanical connection to the bottom or top lids.

Using this method we were able to reach frequency ratios $N/f \approx 2-6$ in our experiments. These, being larger than unity, imply that the IGW propagation is expected to be qualitatively similar to the atmospheric case. An example of the detected short-wavelength, high-frequency wave patterns is

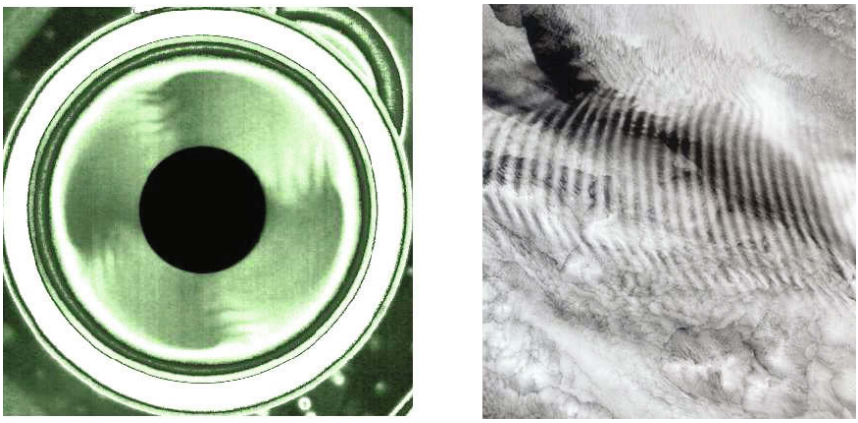

Figure 6. Possible signs of small-scale inertia-gravity wave excitation from the $m = 4$ baroclinic wave pattern (left) and its analogy in the atmosphere (right), as seen from orbit (Source: NASA).

shown in the infrared thermographic image at the left hand side of Figure 6. It is clearly visible that the large-scale fourfold symmetric ($m = 4$) baroclinic waves (anticyclones) radiate away the minor ripples corresponding to the possible surface signatures of IGWs. For a comparison of the structures, an orbital image taken from the International Space Station is presented at the right hand side of Figure 6, showing actual atmospheric IGWs.

The reason of the observed wave emission is probably transient geostrophic imbalance: all the detected IGW-like patterns appeared right after changing rotation rate Ω during the experimental sequence, and vanished within 30 revolutions time, whereas the large-scale baroclinic wave patterns survived throughout the whole measurement period (typically lasting for 2-3 hours or 6-700 revolutions). It is to be remarked that infrared thermography is far not optimal method for IGW detection, since the applied wavelength range can only escape from the uppermost few millimeters below the free water surface, thus everything that could be observed this way are just faint hints of the dynamics in the bulk.

The search for underwater IGW signatures in the rotating annulus will continue with utilizing an array of small digital thermometers and salinity sensors that will be placed into the working fluid, and will log the values with a temporal resolution above 10 Hz. According to numerical results (Borchert et al., 2014; Randriamampianina, 2013) and the above presented

preliminary surface temperature data, the wave filaments appear to be connected to the baroclinic wave lobes. Thus, one would expect that if a baroclinic wave lobe passes by the sensor, amplitude enhancement would appear in the IGW frequency range, i.e. at $f < \omega < N$. The temporal pattern of this modulation itself should therefore be determined by the low-frequency baroclinic wave propagation. The signals of different temporal scales will then be separated and compared via bandpass filtering. These laboratory experiments are currently underway, and will hopefully yield clear experimental evidence of IGW excitation processes in a differentially heated rotating set-up.

3.2 Dynamics of passive tracers in the atmosphere

Anthropogenic emissions often result in pollution levels that exceed air quality standards at many locations over both hemispheres. Air quality and pollutant dispersal are strongly influenced by large scale transport processes at the intercontinental and global scales. Pollutant particles can travel huge distances depending on their size and density, small aerosols can reach the stratosphere and get around the globe several times until falling out. The first approximation for the motion of light particles advected by environmental flows is the approach of "passive tracer" dynamics, where particle size is assumed to be negligible and the density is equal with the surrounding liquid, thus such particles passively follow the flow without disturbing it (see the Chapter by Haszpra and Tél in this volume). Passive tracer dynamics is often studied experimentally by using various dyes (Ewart and Bendiner, 1981; Sommerer et al., 1996; Gouillart et al., 2009), since soluble chemicals hardly affect flow fields especially in the turbulent regime.

Our experiments (Jánosi et al., 2010) were carried out in the classical laboratory model for mid-latitude large-scale flow phenomena, which is a differentially heated rotating annulus invented by Fultz (Fultz, 1949, 1952; Fultz et al., 1959) and Hide (Hide, 1953, 1958; Fowlis and Hide, 1965; Hide and Mason, 1975), and analyzed in details in Subsection 3.1. The setup, also used in (Gyüre et al., 2007) (see Subsection 3.3), consists of three concentric cylinders of radii $R_1 = 4.5$, $R_2 = 15.0$, and $R_3 = 20.3$ cm which is fixed on a rotating platform. The central container is filled up with a mixture of ice and water, the outermost one is regulated by an immersion heater, the working fluid in the middle annular region is tap water in the presented experiments. The main control parameters are the angular velocity $\Omega \in [1.54, 2.31]$ rad/s and imposed radial temperature difference $\Delta T \in [15.0, 40.5]$ °C in the dish. The height of the working fluid H is varied in a narrow range of 3.3-4.0 cm in order to warrant that the dynamics is well inside the geostrophic

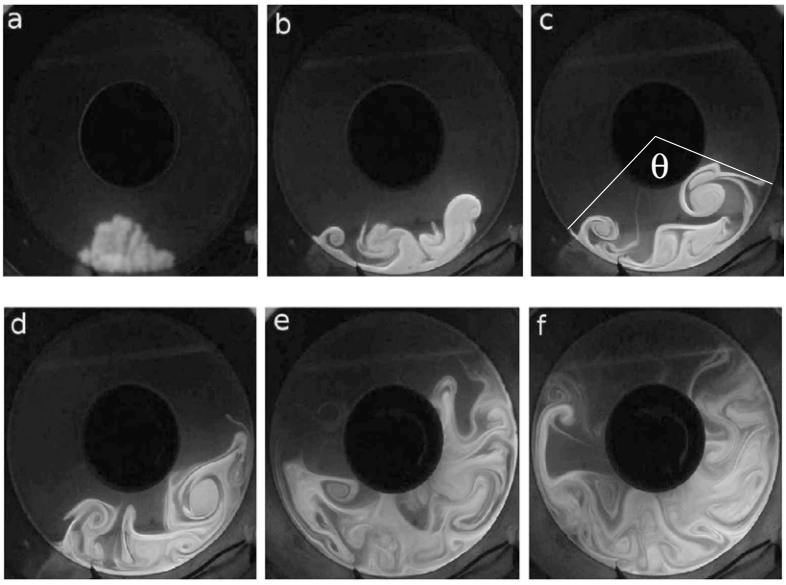

Figure 7. The spread of fluorescent dye as a function of time at parameters $\Delta T = 31.5$ °C, $\Omega = 1.62$ rad/s, $H = 3.4$ cm ($\mathrm{Ro}_T = 0.0209$). (a) 1 s, (b) 8 s, (c) 19 s, (d) 46 s, (e) 120 s, and (f) 154 s after the injection. The angle θ characterizes the zonal range covered by the cloud.

turbulent regime (Hide and Mason, 1975; Salmon, 1998). The convenient nondimensional combination Eq. (3) introduced in Section 2 as thermal Rossby number covers the range $\mathrm{Ro}_T \in [0.01, 0.09]$ with $\alpha \approx 2 \times 10^{-4}$ °C^{-1} for water, and $L = R_2 - R_1 = 0.105$ m.

Fluorescent dye (Sodium fluorescein, $C_{20}H_{10}O_5Na_2$) is used as passive tracer, and dispersion is evaluated by digital image processing (Jánosi et al., 2010). Figure 7 illustrates a typical experiment, where the zonal range of the tracer cloud can be characterized by the time dependent angle $\theta(t)$. Furthermore, the total number of pixels $n(t)$ above a contrast threshold is also determined for each frame. In order to decrease the effects of inhomogeneities of UV illumination, an averaging over one revolution is performed prior to further processing. Note that while $\theta(t)$ is a simple linear measure of tracer dispersal, the time evolution of the total area $n(t)$ is affected by at least three processes with different weights at a particular set of parameters. Chaotic advection by the background flow field continuously increases the

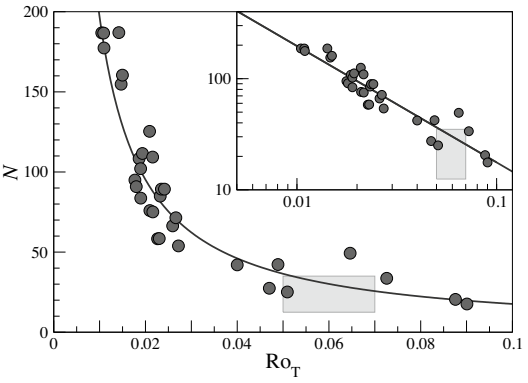

Figure 8. Number of revolutions N until the zonal spread of the dye cloud covers a whole circle as a function of thermal Rossby number Ro_T. The inset shows the same data on a double logarithmic scale. The continuous line is an inverse relationship $N \sim \mathrm{Ro}_T^{-1}$. Shaded rectangle indicates plausible range for the rotating Earth (Jánosi et al., 2010).

colored area, meanwhile local shearing contributes to mixing mostly between vortex walls and cores, however diffusional thinning continuously decreases the fluorescent intensity. Therefore we do not expect that the zonal extent θ obeys a trivial relationship with a composite measure of total cloud size n. The experimental results, served as benchmark for subsequent numerical simulations in Jánosi et al. (2010), can be summarized as follows.

The dominating patterns clearly indicate strong irregular cyclonic and anticyclonic activity (see Fig. 7). It is widely accepted that this dynamics driven by the baroclinic instability reflects the most essential features of mid-latitude atmospheric flow (see Subsection 3.1). The general time evolution for both quantities $\theta(t)$ and $n(t)$ is found to be approximately linear: $\theta(t) = m_\theta(\mathrm{Ro}_T)t+\theta_0$ and $n(t) = m_n(\mathrm{Ro}_T)t+n_0$ with slopes m_θ and m_n depending on the control parameter Ro_T. Linear zonal growth can be followed up to $\theta = 360°$. The growth of total colored area proceeds also to a given time, where a crossover to a constant apparent cloud size is visible (Jánosi et al., 2010). As for the dependence on the control parameter, we obtained a linear relationship for slopes m_θ ($m_\theta \sim \mathrm{Ro}_T$), and a power law $m_n \sim \mathrm{Ro}_T^\delta$ with $\delta \approx 2$ (Jánosi et al., 2010) . Note that we could not find any theoretical prediction for such behavior in the literature available for us.

An interesting quantity to be compared with real observations is the

encompassing time t^* expressed as a dimensionless number $N = t^*\Omega/2\pi$, which is the number of revolutions until the leading and tailing edges of the tracer cloud cross the same "longitude" in the rotating annulus. In order to minimize the effect of different initial configurations, the measured temporal interval of $t(\theta_0 \to 360^\circ)$ is extrapolated to $t(0 \to 360^\circ)$ assuming the same average zonal spreading velocity (here θ_0 is the initial zonal extent of the dye cloud after the injection). The result is plotted in Fig. 8. The relationship is clearly an inverse function $N \sim \mathrm{Ro}_T^{-1}$: the stronger the convective drive the lower the number of revolution until a "hemispheric" encompassing.

If we intend to compare experimental N values with observations, we need an estimate for the thermal Rossby number Ro_T for the rotating Earth. This is not trivial, because of the differential rotation of the Earth (the Coriolis parameter changes with the latitude) and the different thermal boundary conditions (distributed heating of the atmosphere). Still, when we assume that the laboratory setup adequately models mid-latitude atmosphere between 30°-70°, an approximate mean temperature difference can be $\Delta T \approx 25 - 30$°C. Relevant length scales are $H = 10$ km, $L = 4500$ km, a mean Coriolis parameter [replacing 2Ω in Eq. (3)] is $f \approx 10^{-4}$ s^{-1}, and an average coefficient of volumetric expansion for air is $\alpha \approx 4 \times 10^{-3}$ °C^{-1}. An estimated thermal Rossby number [see Eq. (3)] should fall in the range [0.05-0.07]. The range of plausible values for N can be estimated from numerical simulations of passive tracers in reanalysis wind fields (Jánosi et al., 2010). Obtained results represented by the shaded rectangle in Fig. 8 are consistent with the laboratory experiments and thus with the underlying assumptions.

3.3 Asymmetric temperature fluctuations in the atmosphere

Although it is clear that atmospheric dynamics is inherently nonlinear and irreversible, several studies have been suggested that the synoptic-scale activities may be approximated by linear dynamics. Accordingly, strong correlations characterize the dynamics for short time intervals that permits a satisfactory description of atmospheric parameter changes as a low order linear autoregressive process (Király and Jánosi, 2002). Such processes are symmetric under time reversal leading to the 'reversibility paradox' (Loschmidt, 1876): how to deduce an irreversible process from time-symmetric dynamics? Both macroscopic irreversibility and microscopic time-reversal symmetry are well-accepted principles in physics, with solid observational and theoretical support, yet they seem to be in conflict; hence the paradox.

The lack of time-reversal symmetry of temperature fluctuations in labo-

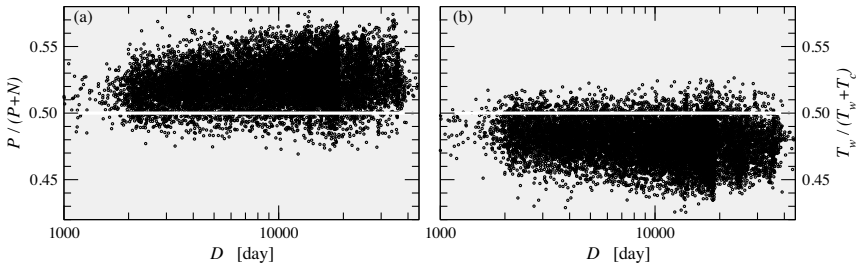

Figure 9. Two asymmetry measures as a function of record length D. (a) The number of positive daily mean temperature steps over the total number of steps $P/(P+N)$, and (b) the ratio $T_w/(T_w+T_c)$ where T_w and T_c denote the mean one-day temperature change of warming and cooling averaged over the total length of a given record. The results for 13380 terrestrial meteorological stations are plotted. (Bartos and Jánosi , 2005; Gyüre et al., 2007; Kiss and Jánosi, 2010)

ratory experiments on turbulent thermal convection is relatively well known (Belmonte and Libchaber, 1996), where the statistics of time derivative of temperature records is found to be an appropriate tool to characterize the dynamics of the flow. The temporal asymmetry is simply quantified by the skewness of magnitude probability density functions. The observed behavior is that the skewness has a positive value at the cold (top) boundary, it changes sign at around the border of the cold thermal boundary layer, and it is increasingly negative for larger distances (Belmonte and Libchaber, 1996). The question naturally arises: is there a similar behavior expected in the atmospheric boundary layer, where thermal convection is also a fundamental constituent of dynamics?

A comprehensive analysis of 13380 daily mean temperature time series from the Global Daily Climatology Network (GDCN, compiled by the National Climatic Data Center) resulted in an apparent time reversal asymmetry considering one day temperature differences. Figure 9a shows that the number of warming steps is definitely larger than the number of cooling steps at almost every terrestrial locations (mostly in the northern midlatitude band) irrespective of the length of the record. Here the simple asymmetry measure $P/(P+N)$ is used, where P and N denote the number of positive and negative steps. This strong asymmetry is necessarily compensated by larger average values for the cooling steps (Fig. 9b), here T_w and T_c are the mean warming and cooling step magnitudes at a given mea-

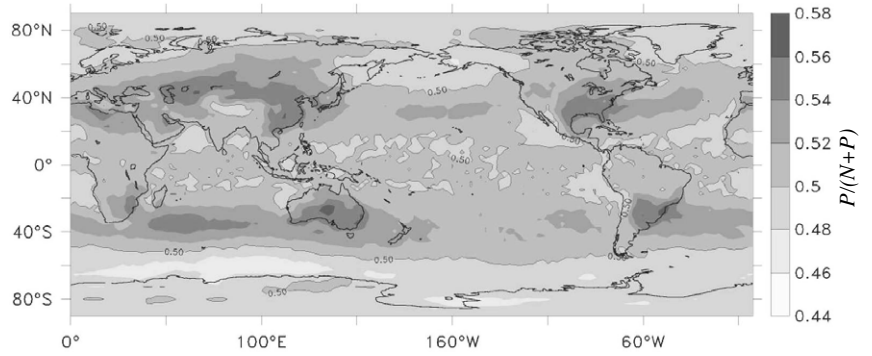

Figure 10. A map of the one-day asymmetry measure $P/(P+N)$, based on the surface daily mean temperature of the NCEP–NCAR reanalysis for the time period 1948–2006. (Ashkenazy et al., 2008; with permission)

suring site. The correlation between the two ratios (warming step number over cooling step number, and mean cooling step size over mean warming step size) is very strong, the computed correlation coefficient has a value of $r = 0.984$. The observed asymmetry is a consequence of higher order nonlinear correlations in the time series demonstrated by Kiss and Janosi (Bartos and Jánosi, 2006; Kiss and Jánosi, 2010).

In a comprehensive follow-up study, Ashkenazy et al. (2008) evaluated 59 years of the NCEP/NCAR (National Centers for Environmental Prediction, and National Center for Atmospheric Research) reanalysis data, including a global, multilevel coverage of temperature with a spatial resolution of 2.5×2.5. The measure of asymmetry they used is based on warming- and cooling-step numbers, too. Apart from the vicinity of the equator, daily surface-temperature fluctuations obey a significant time asymmetry on both hemispheres (Figure 10). The general behavior is that large cooling steps are followed by slower gradual warming. This is a statistical pattern, the temperature records rarely exhibit a very clear sawtooth pattern. The asymmetry changes sign at latitudes around ±60°. At higher latitudes, sudden warming jumps are followed by slower gradual cooling. The asymmetry fades away as a function of altitude indicating clearly the role of atmospheric boundary layer. The asymmetry also fades away when longer-time differences are evaluated, such short-time 'memory' (persistence) of weather phenomena is known to have a characteristic time scale of 4-5 days.

Based on their careful analysis and detailed comparisons with annual

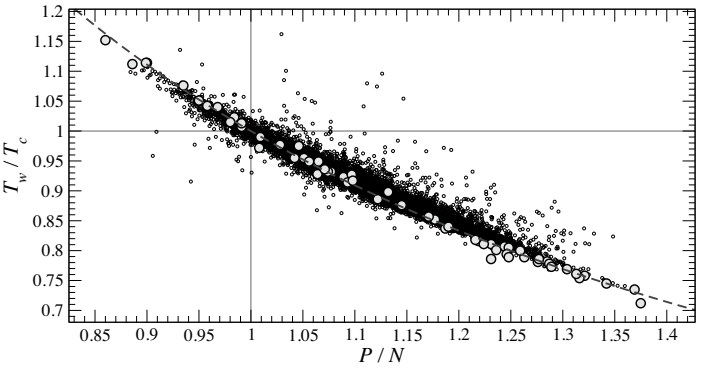

Figure 11. Correlation plot between step number ratio P/N and average step size ratio T_w/T_c for one-day temperature changes. Small cyrcles: 13380 terrestrial weather stations. Large gray circles: laboratory experiments. Dashed line indicates the perfect stationarity condition. (Gyüre et al., 2007)

mean transient heat flux and the frequency of low pressure events (storms), Ashkenazy et al. (2008) formulated a convincing explanation of the observed time reversal asymmetries in daily mean temperature changes. The rapid cooling seen in the mid-latitudes and the rapid warming seen in the high latitudes must be associated with the cold or warm fronts that propagate toward low/high latitudes, correspondingly. After the passage of a cold or warm front, the temperature relaxes to the equilibrium atmospheric temperature, where the (possibly small scale convective, diffusive and radiative) relaxation processes are relatively slow compared to the front propagation. At the mid-latitudes, the temperature slowly relaxes after the passage of the cold front to the warmer equilibrium temperature; at the high latitudes, the temperature slowly relaxes after the passage of the warm front to the colder equilibrium temperature.

Since the main message of this Chapter is that a thermally driven rotating annulus reproduces the basic physics of the mid-latitude atmosphere, it is quite plausible to perform an experimental check of temperature fluctuations. Gyüre et al. (Gyüre et al., 2007) implemented temperature measurements in the classic rotating annulus sketched in Figure 4b. Angular velocities in the range 1.88-4.71 $s^{?10}$ at two temperature gradients were imposed: $T_{w0} = 35.0 \pm 0.1°C$ and $40.0 \pm 0.1°C$ outside, melting ice ($T_{c0} \approx 4°C$) inside. Two corotating Ni-NiCr thermocouples fixed at the end of thin wires of diameter 0.5 mm were sampled at a rate of $\Delta t = 3.0$ s, which is approximately

one sample per revolution, in analogy with the meteorological records. The height of the sensors was fixed at 3 mm from the bottom; the radial positions were changed in the experiments running 5?6 hrs each. In the non-rotating control experiments the presence of simple radial convection was checked, and the typical flow speeds obtained were between 0.5 and 1.0 mm/s. The imposed parameter range is deeply in the dynamical regime of irregular wave patterns (cf. Figure 5), similarly to the mid-latitude atmosphere.

The experimental temperature records were evaluated in the same way as the meteorological data. The same robust asymmetries in the statistics of temperature changes were observed; the results are shown in Figure 9. The apparent data collapse onto the curve of strict stationarity in Figure 11 (dashed line) is somewhat surprising for the meteorological data, which means that systematic baseline drifts (urbanization, changing land use, global warming, etc.) are hardly visible in the records. The simple experimental setup cannot model many fundamental aspects of the real atmosphere, such as the strong density stratification (compressibility), the distributed differential heating by insolation, or the latitude dependent strength of the Coriolis parameter. Still, the marked violation of time reversal symmetry in the experimental tank further strengthens the physical analogy between the geostrophic turbulence observed in the troposphere and the differentially heated rotating annulus.

3.4 Interdecadal climate variability in the laboratory

Atlantic Multidecadal Oscillation (AMO) – a term coined by Kerr (2000) – or as it is more accurately referred to, 'Atlantic Multidecadal Variability' (AMV) is a robust temperature signal in the interdecadal frequency band of the paleoclimate and instrumental records of the North Atlantic region, stretching back to centuries. In the past years, a consensus has been emerging within the community that at least two different, more or less independent processes contribute to this variability: one of 20-30-year and another of 50-70-year characteristic timescales (Dong and Sutton, 2005; Vellinga and Wu, 2004). More radically, it has been suggested (by the authors) that this interdecadal spectral band may not be special by any means after all, but can be interpreted as a realization of the same multi-scale long-range-correlated stochastic dynamics that yields proper fits to the anomalies of much smaller timescales as well (Vincze and Jánosi, 2011).

The importance of AMV's contribution to global climate is immediately visible when comparing the two time series of Figure 12 The top curve shows the instrumental record of the so-called 'AMO index' (AMOI), introduced by Enfield (Enfield et al., 2001), that is defined as the 121-month running

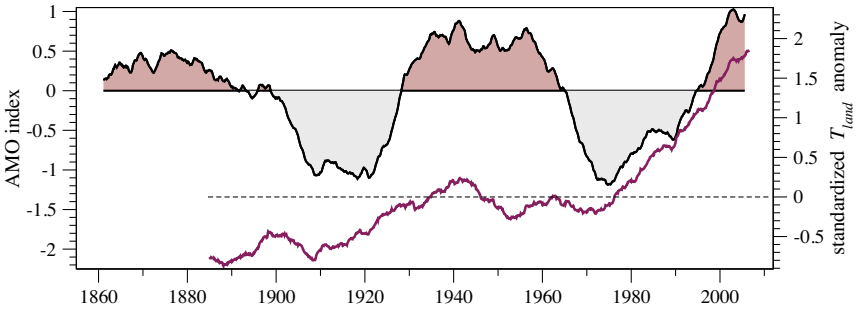

Figure 12. AMO index (left, thin black line) and standardized global mean temperature anomaly over land T_{land} (right, thick black line) shifted downwards for a better visualization. Both records are smoothed by a 121 months running mean filter. Sources: http://www.esrl.noaa.gov/, and http://www.ncdc.noaa.gov/.

mean of sea surface temperature (SST) anomalies, averaged over the North Atlantic basin. The 'warm' 1940s (positive AMOI), and the 'cold' 1970s (negative AMOI) – when climate scientists envisioned the signs of a new ice age – can be clearly distinguished. It is interesting to note that the standardized global mean temperature record over land T_{land} shown by the bottom curve of Figure 12 (shifted downwards for visualization), after the same type of 121-month smoothing, appears to exhibit a rather robust correlation with the AMOI, superposed onto the increasing trend: clearly, AMV is one of the strongest components of mid-latitude climate variability. The phase of AMV also correlates with a certain spatial pattern of the North Atlantic SST field, as reported by Kushnir (Kushnir, 1994). In the AMOI > 0 intervals, SST anomalies are generally positive in the whole basin, except for the coast of Newfoundland, where a localized negative temperature anomaly appears. In the cold phases the sign reverses: an overall cold anomaly develops with a warm domain around Newfoundland.

Although the 'ingredients' of AMV may be numerous and complex, a surprisingly simple conceptual dynamical minimal model has been proposed by te Raa and Dijkstra (2002), which can reproduce several basic features of the 20-30-year 'mode' of the variability. Their model consists of a rotating rectangular sector of a uniform depth ocean and meridional SST gradient. Frankcombe et al. (2009) showed that a multidecadal oscillatory mode can be excited in this arrangement, by adding temporally and spatially cor-

related red noise forcing to the SST field, representing ocean-atmosphere interactions. This model is "minimal", or irreducible in the sense that if any of the three key components (rotation, meridional temperature gradient and thermal noise) is removed, the oscillatory mode can no longer be excited.

After learning about this conceptual numerical model of appealing simplicity from Henk *Dijkstra* in a summer school on climate variability, we decided to construct a laboratory experiment in which its implications can be tested (Vincze et al., 2012). In the apparatus the North Atlantic basin was represented by a rectangular acrylic tank, divided into three sectors by two internal vertical walls, as depicted in Figure 13. The central domain of length $L = 68$ cm and width $D = 25$ cm was filled up to height $H = 10$ cm with tap water. One of the side sectors – separated by a copper internal wall from the central domain – was packed full of melting ice, enough to keep the temperature in this separated compartment at $(0\pm0.1)^\circ$C for up to 5 hours (the average duration of our experimental runs). On the opposing vertical sidewall, an electric heating element was mounted, capable of releasing a maximum flux of 0.3 W cm^{-2}. These two heat sources provided the analogue of the meridional temperature gradient in our setup. The differential heating initiates a "sideways convective" flow (similarly to the rotating annulus experiments of the previous sections): in the absence of critical Rayleigh number, *any* temperature difference ΔT between the sidewalls is sufficient to do so. The apparatus was placed on a turntable, rotating at period $P = (3.0 \pm 0.05)$ s. Nine digital thermometers, placed into the top 1 cm of the working fluid were arranged into an equidistant grid and logged the 'sea surface' temperature values in the tank at a temporal resolution of 1 s^{-1}.

The third key component (besides temperature gradient and rotation) in the minimal model of Frankcombe et al. (2009) is the perturbative effect of a spatially correlated and temporally red noise-like anomalous heat flux at the water surface (representing 'weather'). This 'ingredient' was modeled by a halogen lamp of large infrared emission, mounted 50 cm above the water surface. These heat flux perturbations were on the order of 0.5°C all over the water surface (whereas the values of the 'merdidional' ΔT varied between 0.25 and 1.75°C). The lamp was turned on and off according to a stochastic sequence, controlled by a computer, with a mean time interval $m = 200$ s between subsequent actions, and standard deviation $\sigma = 50$ s. Thus the timescale of thermal forcing was approximately 400 s, or 130 P. Our control experiments demonstrated that indeed all three components are needed to excite low frequency variability in the set-up. If any one of lamp forcing, rotation or sidewall heating/cooling was absent, the low frequency

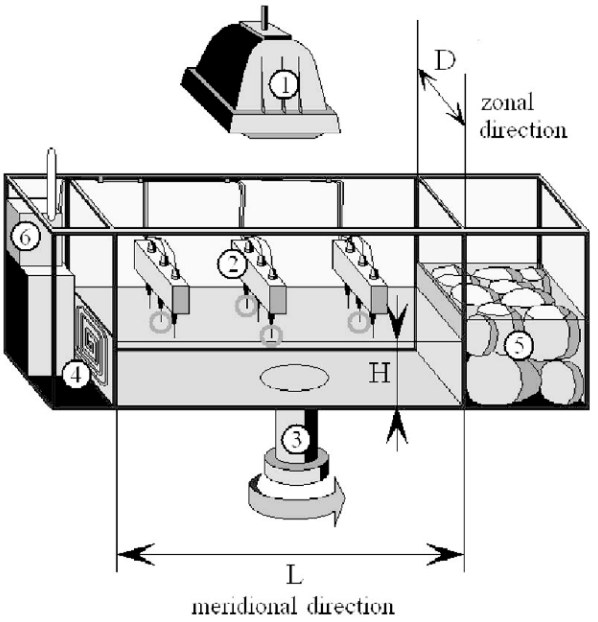

Figure 13. Schematic drawing of the setup. 1: lamp (for the surface heat flux perturbation), 2: digital temperature sensors (nine in total), 3: axis of rotation (the direction of rotation is also indicated), 4: electric heating module ("equator"), 5: the cooling sector packed full of ice ("polar region"), 6: radio transmitter for real time data acquisition. The geometric parameters L, D and H are indicated, together with the corresponding terminology ("zonal" and "meridional") (Vincze et al., 2012).

temperature oscillations disappeared (see Vincze et al. (2012) for details).

Next, using the average 'meridional' temperature difference $\langle \Delta T_M \rangle$, measured between the heated and cooled end of the tank as a control parameter, we evaluated the periods corresponding to the largest spectral amplitude for seven experimental runs at different values of side heating. The periods were acquired from the 'zonal' temperature difference anomalies (δT_Z).

In the minimal model, the period of the low frequency mode is set by the 'patch crossing time' i.e. the time it takes for a SST anomaly to drift across the North Atlantic basin in the zonal direction. In a thermally driven rotating system, an order-of-magnitude estimate of the drift velocity can

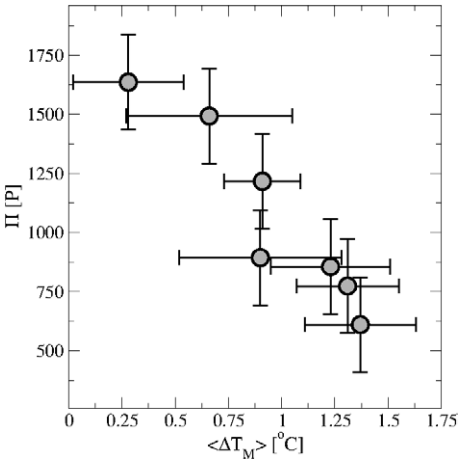

Figure 14. Period of the largest observed Fourier component of the band-pass filtered zonal temperature difference anomalies (δT_Z), as a function of the average meridional temperature difference (Vincze et al., 2012).

be obtained as written in equation (5) of Section 2. From here, one can conclude that the patch crossing time, and hence the period of the oscillatory mode scales with ΔT^{-1}. This assumption fairly agrees with our finding that a clearly decreasing trend can be observed, as visible in Figure 14.

As a "mechanistic indicator" associated with the *spatial pattern* of the multidecadal variability, Dijkstra et al. (2006) proposed to measure the phase lag between east-west and north-south temperature differences. Inspired by this idea we processed the "meridional" and "zonal" temperature difference anomaly signals (δT_M and δT_Z) accordingly. In order to quantify the phase shift between the two time series, cross correlation analysis was conducted with a maximal lag of 5000 s (1667 P); as a rule of thumb we chose the location of the first maximum at a positive lag as a measure of the phase shift.

As mentioned above, the mechanism of the 20-30 year mode of the multidecadal oscillation is supposedly based on the principle of quasi-geostrophic *thermal wind balance*, which enables a meridional temperature anomaly to initiate an anomalous zonal velocity perturbation. This provides an anomalous (perpendicular) component to the meridional overturning background flow, and by doing so, the temperature anomaly is getting pushed towards a meridional sidewall, yielding a zonal temperature gradient, and to the excitation of a meridional overturning anomaly (te Raa and Dijkstra, 2002).

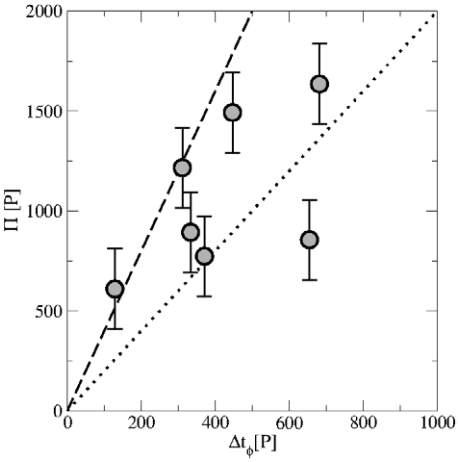

Figure 15. Period of the largest observed Fourier component of the band-pass filtered zonal temperature difference anomalies (δT_Z) as a function of the phase lag between the meridional and zonal temperature difference anomalies (obtained via cross correlation analysis). The dotted line represents $y = 2x$, the dashed line marks $y = 4x$. The fact that most of the data points lie between the two lines, implies positive correlation (Vincze et al., 2012).

This interplay between temperature and velocity anomalies drives the observed pattern formation in the system and sets the timescale of the oscillation. As a consequence of this reasoning, one would expect a correlation between the above discussed zonal-meridional phase lags and the period of the oscillation itself. Figure 15 shows this dependence for seven experimental runs. For each run, the phase lag value was obtained via the aforementioned cross-correlation method. Although the results are not exactly conclusive, yet a clear trend is present: most of the observed phase lags are found to be between quarter and half a period (see dotted and dashed lines in Figure 15). Naturally, for a clear oscillatory mode with one single frequency and one persistent, permanently cycling surface patch (a "thermal Rossby wave"), the phase lag between zonal and meridional temperature differences would be exactly one fourth of a period. However, for a "lamp noise"-induced dynamics present here, it is not surprising at all that the spatial and temporal behavior apperars to be more complex.

4 Concluding remarks

With this chapter, we intended to give the reader an overview on the role that laboratory experimentation has been playing in the development of meteorology, oceanography and climatology since the 18th century, and an insight into some of the current research topics. After discussing the past and the present, the question naturally arises of what kind of impact and contribution this research method can possibly have to the environmental sciences of the near future, marked by the 'digital revolution', the incredible growth of computing capacity available for numerical modeling.

One could of course argue in the spirit of Richard P. Feynman, saying that "experiment is the sole judge of scientific truth" (Feynman, 1967). However, in reference to atmospheric or oceanic dynamics we have to keep in mind that it is not possible to conduct actual experiments on planetary scales: in this sense laboratory experiments are merely incomplete models, just as much (or from many aspects, even more) as numerical simulations.

Thus the answer to the above question is twofold. Firstly, even compared to the best computers, nature itself still possesses the greatest possible computing power. In a properly set experiment, nonlinear phenomena which would require computationally intensive numerical codes to approximately implement, can be readily accessed in real time with practically infinite degrees of freedom. Continuing Feynman's above train of thought: "It always bothers me that according to the laws as we understand them today, it takes a computing machine an infinite number of logical operations to figure out what goes on in no matter how tiny a region of space and no matter how tiny a region of time". Indeed, treating such down-scaled models of continuous media as analog computers, or with the words of Carl-Gustaf *Rossby* (1898–1957) 'mechanical integrators' (Rossby, 1926) is one of the greatest strengths of experimental modeling. This is especially true for systems where wide ranges of spatial and temporal scales are heavily interconnected, and therefore a cut-off in resolution (inevitable in simulations) could significantly alter the observed dynamical behavior.

Secondly, experimental minimal models provide a superb test-bed to tune and validate large and complex 'Nimitz-class' general circulation models (GCMs) of the ocean and the atmosphere, designed for weather forecasts and global climate predictions. Systematic tests of these operational codes are especially hard to perform; separating the inaccuracies that arise due to faulty numerical implementation from the ones originating from our incomplete understanding of the processes of Earth's weather system (e.g. the details of cloud formation, the role of aerosols, etc.) poses a real challenge to researchers. In the laboratory-based systems, however, all governing equa-

tions and boundary conditions are fairly well known and can be adjusted or controlled precisely. Therefore all the errors and deviations that come up when simulating the flow in the experimental set-up using these GCMs cannot be blamed on the complexity of climate, but must be attributed to improper implementation.

As an example, we refer to the German Science Foundation's (DFG) *MetStröm* project (2008–2014), whose primary goal was to realize this very concept. A water-filled differentially heated rotating annulus served as a reference experiment and the model flow was simulated by five different working groups and GCMs, using various numerical approaches, solvers and subgrid-scale parametrization methods (Vincze et al., 2015). The results have uncovered some systematic discrepancies between the majority of the investigated numerical models and the experiment, and led to the refinement of their methods, hopefully contributing to better weather forecasts in the future.

Bibliography

Ashkenazy, Y., Y. Feliks, H. Gildor, and E. Tziperman, *Asymmetry of daily temperature records*, J. Atmos. Sci. **65**, 3327-3336, 2008.

Aubert, O., M. Le Bars, P. Le Gal, and P. S. Marcus, *The universal aspect ratio of vortices in rotating stratified flows: experiments and observations*, J. Fluid Mech. **706**, 34-45, 2012.

Bartos, I., and I. M. Jánosi, *Atmospheric response function over land: Strong asymmetries in daily temperature fluctuations*, Geophys. Res. Lett. **32**, L23820, 2005.

Bartos, I., and I. M. Jánosi, *Nonlinear correlations of daily temperature records over land*, Nonlin. Proc. Geophys. **13**, 571-576, 2006.

Belmonte, A., and A. Libchaber, *Thermal signature of plumes in turbulent convection: the skewness of the derivative*, Phys. Rev. E, **53**, 4893-4898, 1996.

Borchert, S., U. Achatz, and M. D. Fruman, *Gravity wave emission in an atmosphere-like configuration of the differentially heated rotating annulus experiment*, J. Fluid Mech. **758**, 287-311, 2014.

Boschan, J., M. Vincze, I. M. Jánosi, and T. Tél, *Nonlinear resonance in barotropic-baroclinic transfer generated by bottom sills*, Phys. Fluids, **24**, 046601, 2012.

Chen, C. F., D. G. Briggs, and R. A. Wirtz, *Stability of thermal convection in a salinity gradient due to lateral heating*, Int. J. Heat Mass Transport, **14**, 57-65, 1971.

Coman, M. A., Griffiths, R. W., and Hughes, G. O., *Sandström's experiments revisited*, J. Marine Res., **64**, 783-796, 2006.

Delworth, T. L., and R. Greatbatch, *Multidecadal thermohaline circulation variability driven by atmospheric surface flux forcing*, J. Climate, **13**, 1481-1495, 2000.

Dijkstra, H. A., *On the interaction of SST modes in the North Atlantic Ocean*, J. Phys. Oceanogr., **36**, 286-299, 2006.

Dijkstra, H. A., te Raa, L. A., Schmeits, M. and Gerrits, J., *On the physics of the Atlantic Multidecadal Oscillation*, Ocean Dyn., **56**, 36-50, 2006.

Dong, B. and R. T. Sutton, *Mechanism of interdecadal thermohaline circulation variability in a coupled ocean-atmosphere GCM*, J. Climate, **18**, 1117-1135, 2005.

Ekman, V. W., *On dead water*, Norw. N. Polar Exped. 1893-1896: Sci Results, XV, Christiana, 1904.

Enfield, D. B., Mestas-Nunez, A. M. and Trimble, P. J., *The Atlantic Multidecadal Oscillation and its relation to rainfall and river flows in the continental U.S.*, Geophys. Res. Lett., **28**, 2077-2080, 2001.

Ewart, T. E., and W. P. Bendiner, *An observation of the horizontal and vertical diffusion of a passive tracer in the deep ocean*, J. Geophys. Res.: Oceans **86**, 10974-10982, 1981.

Feynman, R., *The Character of Physical Law*, MIT press, 1967.

Fowlis, W. W., and R. Hide, *Thermal convection in a rotating annulus of liquid: effect of viscosity on the transition between axisymmetric and non-axisymmetric flow regimes*, J. Atmos. Sci. **22**, 541-558, 1965.

Frankcombe, L. M., Dijkstra, H. A. and von der Heydt, A., *Sub-surface signatures of the Atlantic Multidecadal Oscillation*, Geophys. Res. Lett., **35**, L19602, 2008.

Frankcombe, L. M., Dijkstra, H. A., and von der Heydt, A., *Noise-induced multidecadal variability in the North Atlantic: excitation of normal modes*, J. Phys. Oceanogr., **39**, 220-233, 2009.

Frankcombe, L. M., von der Heydt, A., and Dijkstra, H. A., *North Atlantic Multidecadal Variability: An investigation of dominant time scales and processes*, J. Climate, **23**, 3626-3638, 2010.

Fultz, D., *A preliminary report on experiments with thermally produced lateral mixing in a rotating hemispherical shell of liquid*, J. Atmos. Sci. **6**, 17-33, 1949.

Fultz, D., *On the possibility of experimental models of the polar-front wave*, J. Atmos. Sci. **9**, 379-384, 1952.

Fultz, D., R. R. Long, G. V. Owens, W. Bohan, R. Kaylor, and J. Weil, *Studies of thermal convection in a rotating cylinder with implications*

for atmospheric motions, Meteor. Monogr. Amer. Meteor. Soc. **4**, 1-104, 1959.

Ghil, M., P. L. Read, and L. A. Smith, *Geophysical flows as dynamical systems: The influence of Hide's experiments*, Astron. Geophys. **51**, 28-35, 2010.

Gouillart, E., O. Dauchot, J.-L. Thiffeault, and S. Roux, *Open-flow mixing: experimental evidence for strange eigenmodes*, Phys. Fluids, **21**, 023603, 2009.

Gyüre, B., I. Bartos, and I. M. Jánosi, *Nonlinear statistics of daily temperature fluctuations reproduced in a laboratory experiment*, Phys. Rev. E, **76**, 037301, 2007.

Hide, R., *Some experiments on thermal convection in a rotating liquid*, Q. J. Roy. Met. Soc. **79**, 161, 1953.

Hide, R., *An experimental study of thermal convection in a rotating liquid*, Phil. Trans. Roy. Soc. Lond. A, **250**, 441-478, 1958.

Hide, R., and P. J. Mason, *Sloping convection in a rotating fluid*, Adv. Phys. **24**, 47-100, 1975.

Holton, J. R., *An introduction to dynamic meteorology*, 4th ed., Academic Press, Burlington, 2004.

Jánosi, I. M., P. Kiss, V. Homonnai, M. Pattantyús-Ábrahám, B. Gyüre, and T. Tél, *Dynamics of passive tracers in the atmosphere: laboratory experiments and numerical tests with reanalysis wind fields*, Phys. Rev. E, **82**, 046308, 2010.

Kaplan, A., Cane, M., Kushnir, Y., Clement, A., Blumenthal, M. and Rajagopalan, B., *Analyses of global sea surface temperature 1856-1991*, J. Geophys. Res. **103**, 567,589, 1998.

Kerr, R. A., *A North Atlantic climate pacemaker for the centuries*, Science, **288**, 1984-1985, 2000.

Király, A., and I. M. Jánosi, *Stochastic modeling of daily temperature fluctuations*, Phys. Rev. E, **65**, 051102, 2002.

Kiss., P., and I. M. Jánosi, *Time-asymmetric fluctuations in the atmosphere: daily mean temperatures and total-column ozone*, Phil. Trans. R. Soc. A, **368**, 5721-5735, 2010.

Klein, M., T. Seelig, M. V. Kurgansky, A. Ghasemi V., I. D. Borcia, A. Will, E. Schaller, C. Egbers, and U. Harlander, *Inertial wave excitation and focusing in a liquid bounded by a frustum and a cylinder*, J. Fluid Mech. **751**, 255-297, 2014.

Kundu, P. K., and Cohen, I. M., *Fluid Mechanics*, 4th revised ed., Academic Press, 2008.

Kushnir, Y., *Interdecadal variations in North-Atlantic sea-surface temperature and associated atmospheric conditions*, J. Climate, **7**, 141-157, 1994.

Lorenz, E. N., *The mechanics of vacillation*, J. Atmos. Sci. **20**, 448-465, 1963.

Lorenz, E. N., *The Nature and Theory of the General Circulation of the Atmosphere*, World Meteorological Organization, 1967.

Loschmidt, J., *Über den Zustand des Wärmegleichgewichtes eines Systems von Körperen mit Rücksicht auf die Schwerkraft, 1. Teil*, Sitzungsber. Kais. Akad. Wiss. Wien, Math. Naturwiss. **73**, 128-142, 1876.

Mann, E., Z. Zhang, S. Rutherford, R. S. Bradley, M. K. Hughes, D. Shindell, C. Ammann, G. Faluvegi, and F. Ni, *Global signatures and dynamical origins of the little ice age and medieval climate anomaly*, Science, **326**, 1256-1260, 2009.

Marsigli, C. L. F., *Histoire physique de la mer*, translated by Leclerc, Amsterdam, 1725.

Mitchell, D. M., L. Montabone, S. Thomson, and P. L. Read, *Polar vortices on Earth and Mars: A comparative study of the climatology and variability from reanalyses*, Q. J. Roy. Met. Soc. **141**, 550-562, 2015.

Oster, G., and M. Yamamoto, *Density gradient techniques*, Chem. Rev., 1963, 63 (3), pp 257-268, 1963.

Ou, H., *A minimal model of the Atlantic Multidecadal Variability: its genesis and predictability*, Climate Dynamics, **38**, 775-794, 2012.

Raa, te L. A., and H. A. Dijkstra, *Instability of the thermohaline circulation on interdecadal time scales*, J. Phys. Oceanography, **32**, 138-160, 2002.

Randriamampianina, A., *Inertia gravity waves characteristics within a baroclinic cavity*, Compt. Rend. Mecanique, **341**, 547-552, 2013.

Rossby, C. G., *On the solution of problems of atmospheric motion by means of model experiments*, Mon. Weather Rev., **54**, 237-240, 1926.

Salmon, R., *Lectures on Geophysical Fluid Dynamics*, Oxford University Press, Oxford, 1998.

Sandström, J. W., *Dynamische Versuche mit Meerwasser (Dynamical experiments with seawater)*, Annal. Hydrogr. Marit. Meteorol. **36**, 6-23, 1908.

Sinha, B. and Topliss, B., *A description of interdecadal time-scale propagating North Atlantic sea surface temperature anomalies and their effect on winter European climate, 1948-2002*, J. Climate, **19**, 1067-1079, 2006.

Sommerer, J. C., H. C. Ku, and H. E. Gilreath, *Experimental evidence for chaotic scattering in a fluid wake*, Phys. Rev. Lett. **77**, 5055-5058, 1996.

Stommel, H., *Thermohaline convection with two stable regimes of flow*, Tellus, **13**, 224-230, 1961.

Sutton, R. T., and Hodson D. L. R., *Atlantic Ocean forcing of north American and European summer climate*, Science, **309**, 115-118, 2005.

Taylor, G. I., *Stability of a viscous liquid contained between two rotating cylinders*, Phil. Trans. Roy. Soc. A, **223**, 289-343, 1923.

Vallis, G. K., *Atmospheric and Oceanic Fluid Dynamics - Fundamentals and Large-Scale Circulation*, Cambridge University Press, Cambridge, 2006.

Vellinga, M. and P. Wu, *Low-latitude freshwater influence on centennial variability of the Atlantic thermohaline circulation*, J. Climate, **17**, 4498-4511, 2004.

Vettin, F., *Experimentelle Darstellung von Luftbewegungen unter dem Einfluss von Temperatur-Unterschieden und Rotations-Impulsen*, Z. Meteor. **1**, 227-230, 1884.

Vincze, M. and I. M. Jánosi, *Is the Atlantic Multidecadal Oscillation (AMO) a statistical phantom?* Nonlin. Processes Geophys., **18**, 469-475, 2011.

Vincze, M., A. Várai, E. Barsy, and I. M. Jnosi, *The effect of a localized geothermal heat source on deep water formation*, Nonlin. Processes Geophys. **18**, 841-847, 2011.

Vincze, M., I. M. Jánosi, E. Barsy, T. Tél, and A. Várai, *An experimental study of the Atlantic variability on interdecadal timescales*, Nonlin. Processes Geophys. **19**, 335-343, 2012.

Vincze, M., S. Borchert, U. Achatz, Th. von Larcher, M. Baumann, C. Liersch, S. Remmler, T. Beck, K. Alexandrov, Ch. Egbers, J. Froehlich, V. Heuveline, S. Hickel, and U. Harlander, *Benchmarking in a rotating annulus: a comparative experimental and numerical study of baroclinic wave dynamics*, Meteorol. Z. **23**, 611-635, 2015.

Walker, J. M., *Farthest north, dead water and the Ekman spiral*, Weather, **46**, 158-164, 1991.

Hepeng Zhang, H., B. King, and H. L. Swinney, *Resonant generation of internal waves on a model continental slope*, Phys. Rev. Lett. **100**, 244504, 2008.